ARTICLE
Journal of Cellular Biochemistry 105:1451–1460 (2008)

Journal of Cellular Biochemistry

Methylene Blue-Mediated Photodynamic Therapy Induces Mitochondria-Dependent Apoptosis in HeLa Cell

Yan Lu,[1] Ruiqing Jiao,[1] Xiaoping Chen,[1] Jieying Zhong,[1] Jianguo Ji,[2] and Pingping Shen[1*]

[1] *State Key Laboratory of Pharmaceutical Biotechnology, School of Life Sciences, Nanjing University, Nanjing 210093, China*

[2] *Proteome Group National Laboratory of Protein Engineering and Plant Genetic Engineering, College of Life Sciences, Peking University, Beijing 100871, China*

ABSTRACT

Methylene blue (MB), a widely studied reagent, is investigated in this work for its usage in photodynamic therapy (PDT). PDT has been proved to be highly effective in the treatment of different types of cancers. Previous studies showed MB has both high affinity for mitochondria and high photodynamic efficiency. To elucidate the effects of MB in PDT, we analyzed PDT-induced apoptosis in HeLa cells by introducing different doses of MB into the culture media. Our data showed that MB-mediated PDT triggered intense apoptotic cell death through a series of steps, beginning with photochemical generation of reactive oxygen species. The release of cytochrome *c* and activation of caspase-3 indicated that MB-PDT-mediated apoptosis in HeLa cells was executed by the mitochondria-dependent apoptotic pathway. Importantly, proteomic studies confirmed that expression levels of several mitochondrial proteins were altered in MB-PDT-induced apoptosis, including TRAP1, mitochondrial elongation factor Tu and peroxiredoxin 3 isoform b. Western blot data showed that phosphorylation of ERK1/2 and PKA were reduced in MB-PDT treated cells, indicating several signal molecules participating in this apoptotic cascade. Moreover, MB-PDT induced an increase in the strength of interaction between Bcl-xL and dephosphorylated Bad. This led to loss of the pro-survival function of Bcl-xL and resulted in mitochondria-mediated apoptosis. This study provides solid evidence of a strong induction by MB-PDT of a mitochondria-dependent apoptosis cascade in HeLa cells. J. Cell. Biochem. 105: 1451–1460, 2008.

KEY WORDS: APOPTOSIS; METHYLENE BLUE; HELA CELL; PHOTODYNAMIC THERAPY; MITOCHONDRIA PROTEOMICS

Photodynamic therapy (PDT) is an established treatment for cancer that involves the systematic or local administration of a tumor-localizing photosensitizer and the irradiation of the targeted lesion with light at appropriate wavelength [Dougherty et al., 1998]. This multi-step procedure initiates a complicated photochemical reaction to generate reactive oxygen species (ROS) [Henderson and Doughterty, 1992]. The cytotoxic products generated by PDT trigger a cascade of molecular events that inactivate cancer cells through apoptosis and/or necrosis [Almeida et al., 2004], which are responsible for tumor degeneration. In the study of Agostinis et al., Bcl-2 phosphorylation following PDT with Hypericin may be a signal in G2/M phase-arrested HeLa cells which was provoked by photodamage to the microtubule network [Vantieghem et al., 2002]. Therefore, PDT has been indicated as a promising treatment for a diverse array of cancers, such as cervical cancer, oesophageal cancer, head and neck cancer, and skin malignancies [Reynolds, 1997; Manyak et al., 1998; Hopper, 2000; Dolmans et al., 2003].

Methylene blue (MB), a member of the phenothiazinium family, is a photosensitizer with extraordinary photochemical properties to

Abbreviations used: 2-DE; two-dimensional electrophoresis; 7-ADD; 7 amino-actinomycin D; ANP32A; acidic nuclear phosphoprotein 32a; DCFH-DA; 2,7-dichlorodihydrofluorescein diacetate; DHR123; dihydrorhodamine 123; ERK1/2; extracellular signal-regulated protein kinase; Gi3 protein; guanine nucleotide binding protein (G protein); inhibiting activity polypeptide 3 protein; GSH; glutathione; HSP90; 90-kDa heat shock protein; MB; methylene blue; PARP; poly(ADP-ribose) polymerase; PDT; photodynamic therapy; PKA; protein kinase A; ROS; reactive oxygen species; TRAP1; tumor necrosis factor receptor-associated protein 1.

Additional Supporting Information may be found in the online version of this article.

Grant sponsor: Ministry of Education of the People's Republic of China; Grant number: NCET-06-0445; Grant sponsor: Ministry of Science and Technology of the People's Republic of China; Grant number: 2006CB910103.

*Correspondence to: Prof. Pingping Shen, State Key Laboratory of Pharmaceutical Biotechnology, School of Life Sciences, Nanjing University, Nanjing 210093, China. E-mail: ppshen@nju.edu.cn

Received 6 July 2008; Accepted 12 September 2008 • DOI 10.1002/jcb.21965 • 2008 Wiley-Liss, Inc.

Published online 3 November 2008 in Wiley InterScience (www.interscience.wiley.com).

have already been applied in PDT. MB is able to yield high quantum intersystem crossing and generate singlet oxygen ($^1O_2$) [Tuite and Kelly, 1993]. It can also produce radical species in the presence of reducing agents [Gabrielli et al., 2004; Tardivo et al., 2005]. In addition, MB can easily cross the cell membrane and anchor mitochondria [Gabrielli et al., 2004], Lysosomes [Yao and Zhang, 1996] and double-stranded DNA [Zhang and Tang, 2005]. Overall, MB-PDT has been demonstrated to exhibit phototoxicity affecting a variety of tumor cell lines in vitro, including adenocarcinoma [Bellin et al., 1961], bladder carcinoma [Gill et al., 1987] and HeLa cervical tumor [Schmidt et al., 1991]. Kirszberg et al. [2005] reported that methylene blue is more toxic to erythroleukemic cells than to normal peripheral blood mononuclear cells. This suggests that MB has different toxicity in normal cells compared to carcinoma cells. MB is already clinically used in PDT, for instance, basal cell carcinoma, Kaposi's Sarcoma, melanoma, virus and fungal infections treatment in some countries, and its use has been shown to be safe in humans [Tardivo et al., 2005]. Although the derivative of MB induces apoptosis in several cell lines [Ball et al., 1998], mechanism of apoptosis by MB-PDT is limited to an understanding only of its role in DNA damage and ROS generation [Noodt et al., 1998; Rodrigues et al., 2007]. The mechanisms of mitochondria participation in cellular apoptosis and the related signal transduction cascade are still unclear. Thus, understanding the molecular mechanisms of apoptosis induced by MB-PDT will provide better understanding of PDT in cancer therapy.

In the current study, we demonstrated that MB-PDT could induce cell killing primarily by apoptosis. Furthermore, Western blot analyses of caspases and cytochrome *c*, along with evaluation of mitochondrial transmembrane potential, provided convincing arguments for the activation of a mitochondria-mediated apoptosis pathway, which was activated by ROS generated by MB-PDT. We also used proteomics to select and analyze the difference in protein expression between control cells and cells induced by MB-PDT on a larger scale. Western blot and co-immunoprecipitation identified several signaling molecules that participate in this apoptotic cascade. The results suggested that MB-PDT induced the down-regulation of a series of phosphorylated proteins, ERK1/2, PKA. This resulted in Bad dephosphorylation, the subsequent increase of the level of Bcl-xL associated with Bad, rapid release of cytochrome *c* into cytosol and the activation of caspase-3, which is the effector molecule to initiate the apoptosis.

RESULTS

HELA CELL APOPTOSIS IS INDUCED BY MB-PDT

To evaluate whether MB-PDT had an apoptotic effect on HeLa cells, we used the DNA dye 7 amino-actinomycin D (7-ADD) assay to determine the phototoxicity of PDT with different concentrations of MB. Shown in Figure 1A, a dose-dependent effect of MB-PDT on cell death was observed. About 78.9% cells died when treated with MB-PDT at 20 M. Cells treated by MB alone (without irradiation and with environmental illumination) showed a lower apoptotic rate than that of MB-PDT group, suggesting that MB-PDT is more toxic to tumor cell lines than MB alone. However, the difference between MB alone and MB-PDT at the concentration of 20 M was not significant, which indicated obvious dark-toxicity of MB at high concentrations that was PDT-independent. Furthermore, the MB at 20 M without environmental illumination showed almost the same cell death percentage as the MB with environmental illumination (Fig. 1A), so the effect of unavoidable environmental illumination was not considered in the other experiments.

Hoechst stain was also used to verify the HeLa cell apoptosis. Considerable nuclear fragmentation was observed when cells were treated with MB at various concentrations, except the lowest one (5 M, Fig. 1B).

Stages of cell apoptosis were distinguished by annexin V and PI binding assays followed by flow cytometry (Fig. 1C) [Cordoba et al., 2005]. MB-PDT induced a dose-dependent increase in apoptosis in HeLa cells: 53.22% of the cells were at early apoptosis phase when MB-PDT was at 20 M, compared with 2.56% of the untreated control. Only a small percentage of cells were observed to be at later stage of apoptosis or necrosis in all treated or untreated groups.

APOPTOSIS INDUCED BY MB-PDT IS RELATED TO MITOCHONDRIA

After MB-PDT induced apoptosis was verified, we tested the release of cytochrome *c*, which is an important indicator of mitochondrial destruction and initiation of apoptosis. Increasing amounts of cytochrome *c* translocated to the cytoplast after cells were treated with MB-PDT (Fig. 2A). It suggested that MB-PDT destroyed mitochondrial membrane. In addition, poly (ADP-ribose) polymerase (PARP), an intracellular substrate of caspase-3, was shown to be cleaved from 116- to 85-kDa fragments, which was most dramatic in cells treated by PDT with 20 M MB (Fig. 2B). The release of cytochrome *c* and activation of caspase-3 indicated that MB-PDT-mediated apoptosis in HeLa cells was executed by the intrinsic apoptotic pathway.

In mitochondria, cytochrome *c* plays an essential role in the generation of mitochondrial transmembrane potential () [Waterhouse et al., 2001]. Release of cytochrome *c* observed in HeLa cells prompted us to evaluate the alteration in mitochondrial transmembrane potential by fluorochrome 3,3-dihexyloxacarbocyanine iodide (DiOC6) staining. As shown in Figure 2C, DiOC6 incorporation was less abundant in the MB-PDT-treated cells than non-treated cells, indicating that MB-PDT reduced the mitochondrial membrane potential. Loss of mitochondrial transmembrane potential due to the disruption of the mitochondrial membrane is characteristic in the mitochondrion-dependent apoptotic pathway [Furre et al., 2005]. The decreased suggests the involvement of mitochondria in MB-PDT induced apoptosis, which further confirms the involvement of mitochondria in MB-PDT treated cells.

OXIDATIVE STRESS PRODUCED BY MB-PDT PLAYS AN ESSENTIAL ROLE IN APOPTOTIC CELL DEATH

Previous research has demonstrated that PDT generates reactive oxygen species, which initiates tumor ablation action, resulting in apoptotic cell death [Tuite and Kelly, 1993; Manyak et al., 1998; Hopper, 2000; Dolmans et al., 2003]. Therefore, we tested the induction of oxidative stress in HeLa cells and its role in regulating MB-PDT-mediated apoptosis. ROS production was measured by dihydrorhodamine 123 (DHR123) and 2,7-dichlorodihydrofluorescein diacetate (DCFH-DA). In MB-PDT treated group (MB

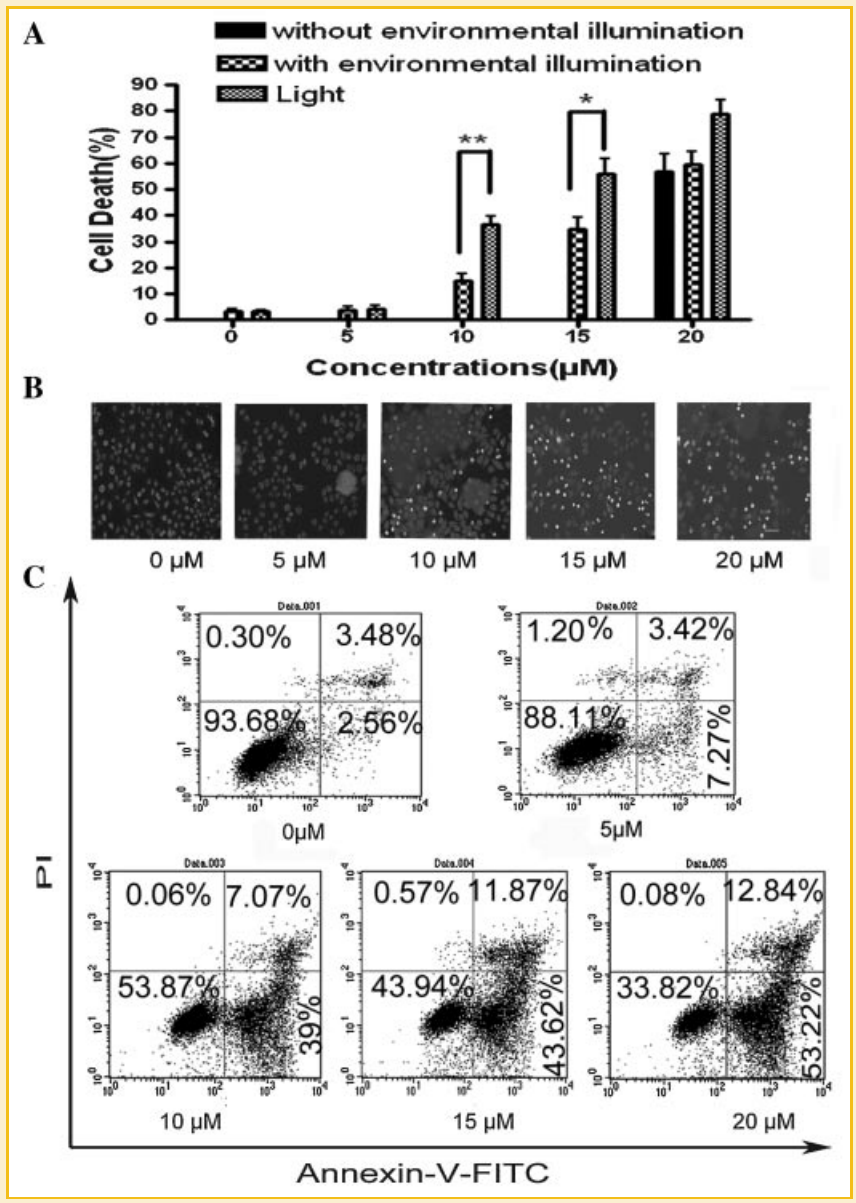

Fig. 1. Cell death analyses of PDT with MB of various concentrations HeLa cells were subjected to PDT treatment described previously with MB of various concentrations as indicated. Analyses were performed 24 h after irradiation. A: Percentage of cell death measured by 7-aminoactinomycin D (7-AAD) analysis. Cells were resuspended in 200 ml binding buffer at a concentration of 10^6 cell/ml. Cells were then incubated with 7-AAD in the dark for 30 min at room temperature and diluted with 400 ml of binding buffer for flow cytometry analysis. The cells incubation with environmental illumination underwent the same process except irradiation. But the cells incubation with 20 M MB without environmental illumination was finished in darkroom to avoid the light. Data represent at least three independent experiments. Asterisks denote a response that was significantly different from the control ($^*P < 0.05$, $^{**}P < 0.01$). B: HeLa cells after Hoechst staining. Cells were fixed, washed once with PBS and stained with Hoechst 33258, then examined with a fluorescence microscopy (40×) connected to cooled CCD image analyzer (Olympus, Tokyo, Japan). Bar, 100 m. C: Flow cytometry analysis of cell preparation stained with Annexin-V and PI. Cells (1×10^6) were washed twice in cold PBS buffer and resuspended in 400 ml binding buffer. The cell suspensions were incubated with annexin V and PI at room temperature in the dark for 20 and 10 min. Cells were analyzed by flow cytometry immediately. Apoptotic cells were detected in the lower right quadrant and necrotic cells in the upper right quadrant.

concentrations ranging from 5 to 20 M), the fluorescence was detected in more than 75% cells with DHR123 ($P < 0.01$), as shown Figure 3A. In contrast, the percentage of fluorescence signals in the cells with MB alone was lower. The intensity of DCFH-DA fluorescence was significantly enhanced ($P < 0.01$) in MB-PDT treated group (MB concentrations ranging from 5 to 20 M) compared with light only group, as shown by the dose–response curves (Fig. 3B).

If MB-PDT induced apoptosis is the outcome of oxidative stress, we would expect to see depressed susceptibility to induce apoptosis when HeLa cells are pretreated with antioxidant (exogenous GSH). Consistent with this prediction, we found that the ratio of apoptosis

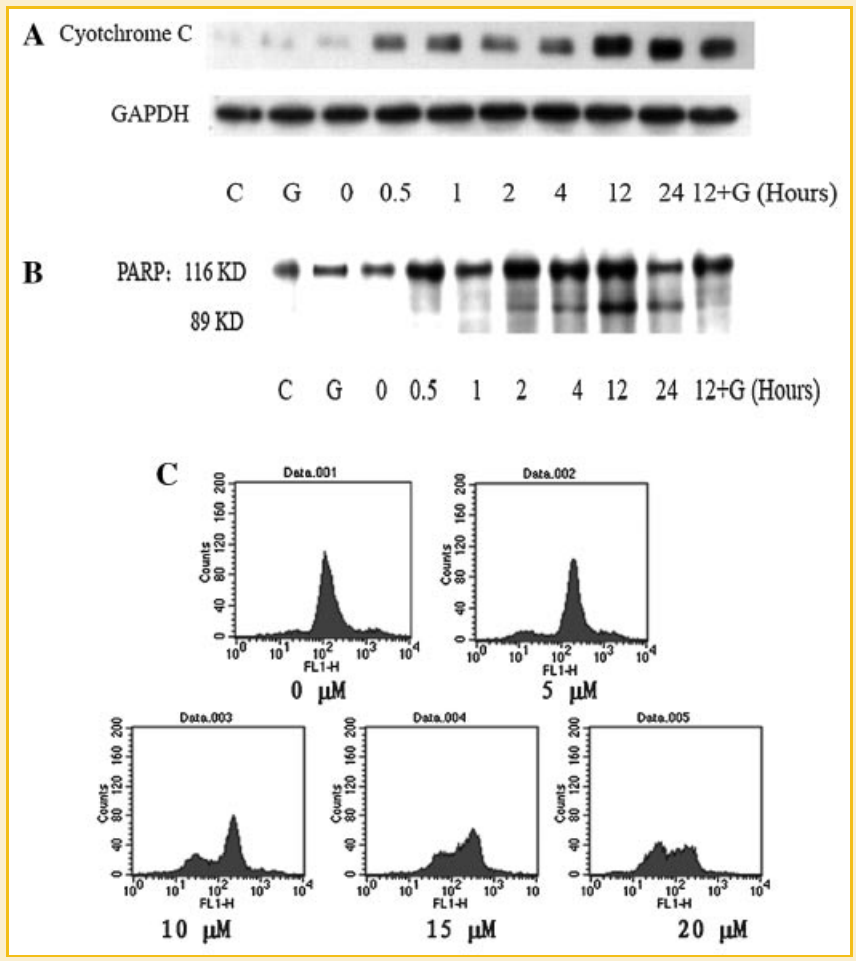

Fig. 2. Apoptosis Induced by MB-PDT related with mitochondria cells were treated with PDT as described previously. Protein was extracted at indicated times after the PDT treatment then subjected to Western blotting using anti-cytochrome *c* antibody (A) and anti-PARP antibody (B), respectively. The figure is representative of at least three separate experiments. C: Cells underwent PDT treatment with MB of various concentrations as indicated. Twenty-four hours after treatment, cells were loaded with DiCO6 (15 g/l) in RPMI-1640 medium for 40 min at 37°C in the dark and then subjected to FACSCalibur flow cytometery analysis.

between MB-PDT treated and untreated samples in the presence of GSH was at least 50% lower than that without GSH, indicating that addition of exogenous GSH partially rescued apoptotic cell death caused by MB-PDT (20 M) (Fig. 3C). On the contrary, as Figure 3D showed, GSH could not protect HeLa cell treated with MB alone from apoptosis, which suggested other mechanism in MB alone. Thus, these observations demonstrated that MB-PDT-mediated activation of cell death is caused by oxidative stress resulting from an imbalance between ROS generation and degeneration.

ANALYSIS OF THE ALTERATIONS IN PROTEIN EXPRESSION INDUCED BY MB-PDT USING PROTEOMICS

Disruption of mitochondrial transmembrane potential observed in MB-PDT treated cells indicated mitochondrial dysfunction during the treatment. In order to provide molecular evidence for mitochondrial dysfunction in response to MB-PDT, we performed a comprehensive proteomics study to identify alterations in protein expression upon the treatment.

The proteomes of the four stages of apoptosis were compared using 2-DE. Three gels per sample were processed simultaneously. Coomassie blue-stained 2-DE gel images were acquired with an image scanner (shown in Supplement Fig. 1A–E) and subsequently subjected to visual assessment to detect changes in protein expression levels and analyzed with PDQuest software. Fifty-one spots were tested, 21 of which were up-regulated and 11 were down-regulated. These identified proteins were involved in protein metabolism; RNA metabolism; signal transduction and oxidative stress (Supplement Fig. 1F). Thirty-two of differentially expressed proteins in MB-PDT treatment are listed in Table I.

The expression level of proteins in charge of mitocondria protein synthesis (TRAP1), electron transfer (mitochondrial elongation factor Tu) and resistance of oxidative stress (peroxiredoxin 3 isoform b) were reduced. Increase of some apoptosis regulation proteins, such as ANP32A and Gi3, affected the synthesis of protein in mitocondria and the transduction of apoptotic signal. These observations revealed that MB-PDT induced apoptosis in HeLa cells involved the mitocondria pathway. Gi3 and ANP32A suppressed the ERK/MEK

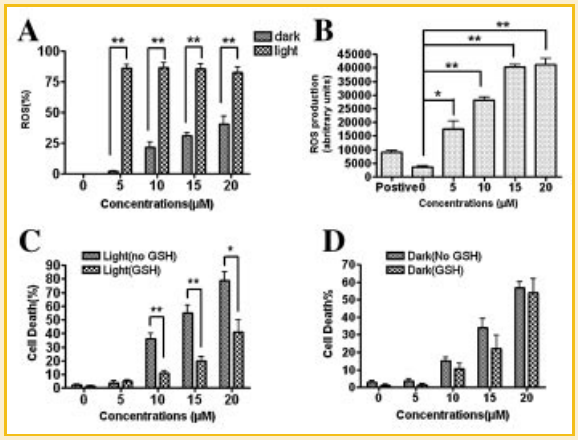

Fig. 3. Effect of intracellular ROS on cell death PDT treatment was performed as described in Materials and methods (A–C) or without irradiation (A,D). A: Cells were incubated with 5 mM DHR123, were washed twice and resuspended in PBS. The fluorescence intensity quantification was measured by FACSCalibur flow cytometery. Intracellular ROS level was measured in 0 h after treatment. B: Cells were incubated with 10 M DCFH-DA, were washed twice and resuspended in medium. The fluorescence intensity quantification as analyzed by a microplate reader after irradiation. In both conditions (C,D), the percentage of cell death was determined by 7-AAD staining in the presence and absence of antioxidant GSH (50 mM), respectively. The histogram is representative of at least three separate experiments. Asterisks denote a response that was significantly different from the control ($^{*}P < 0.05$, $^{**}P < 0.01$).

pathway and phosphorylation of Bad [Valenti et al., 1998; Yu et al., 2004]. However, enzymes, such as phosphatase 2A, acid phosphatase isoenzyme Cf, and phosphatases globally were up-regulated upon MB-PDT treatment, indicating that suppression of PKA, ERKs/MEK activation is an important regulator in the apoptotic process induced by MB-PDT.

IDENTIFICATION OF SEVERAL SIGNAL MOLECULES PARTICIPATING IN APOPTOSIS INDUCED BY MD-PDT

Based on the results of the proteomics, Western blot and co-immunoprecipitation experiments were performed to identify several signaling molecules participate in this apoptotic cascade. The reduction of Phosphorylation levels of ERK1/2 and PKA in a time-dependent manner indicated suppression of PKA and ERK1/2 activation after the cells were treated with MB-PDT (Fig. 4A,B). However, phosphorylation levels of ERK1/2 and PKA were increased by adding GSH when compared with the test of 12 h (Fig. 4A,B), suggesting that dephosphorylation of ERK1/2 and PKA was induced by ROS.

Co-immunoprecipitation was used to analyze the interaction between Bcl-xL and Bad whose phosphorylation was controlled by ERK1/2 and PKA pathway [Klumpp and Krieglstein, 2002; Horbinski and Chu, 2005]. The phosphorylation level of Bad was significantly up-regulated immediately after the treatment of PDT (at 0 h, Fig. 4C), and then started to decrease at 0.5 h, and was gradually inhibited from 2 to 24 h. Accordingly, more Bcl-xL was observed to interact with Bad from 0.5 to 24 h, but the total expression of Bad and Bcl-xL by Western blot were not changed obviously which exclude the influence from protein synthesis (Fig. 4C). The whole results indicated that the interaction between Bcl-xL and Bad increased reciprocally to the reduction of Bad phosphorylation. But when assayed at 12 h, no obvious increase of Bad phosphorylation with GSH was observed, which may be due to the choice of time point.

DISCUSSION

Recently, research on the treatment of malignancy by MB-PDT implied the toxicity of MB to tumor cells and tissue model [Bellin et al., 1961; Gill et al., 1987; Schmidt et al., 1991]. This article discusses the apoptosis and signal transduction pathway induced by MB-PDT. Our study revealed that MB-PDT could induce intense apoptosis of HeLa cells in a dose-dependent manner. PDT plus 20 M MB induced approximate 53.22% of the HeLa cells to undergo apoptosis. Necrotic cells that could induce chronic inflammation and promote tumor growth [Vakkila and Lotze, 2004] only represent 12.48% of the total cells (shown in Fig. 1C). Moreover, our results indicate that the toxicity of MB in the dark is at a low concentration of less than 15 m, which is in good agreement with the previous studies [Orth et al., 2000]. Furthermore, the increase of intracellular ROS and protective effect of adding GSH were not obvious in cell with MB alone, which suggested ROS did not play a major role in the toxicity of MB in the dark.

A critical early event in the apoptosis initiation by MB-PDT is the induction of oxidative stress [Buytaert et al., 2007]. Here, we demonstrated that there was substantial and instant accumulation of ROS in tumor cells challenged with MB-PDT as exhibited by a dose–response curve, which was consistent with the concentration-dependent effects on apoptosis in HeLa cells. Generation and accumulation of ROS associated with MB-PDT caused cell death which can be reversed by adding GSH. These observations suggested that the ROS produced by MB-PDT is an initiation signal of apoptosis in this model.

This article is the first to perform large-scale proteomic analyses to show that MB-PDT led to changes in the abundance of several critical proteins. Among them, reduction of mitochondrial elongation factor Tu, mitochondrial elongation factor Ts and electron transfer flavoprotein (Table I) were observed. Tu and Ts proteins maintain the basic mitochondrial functions, such as the synthesis of 13 polypeptides of the electron transport chain and the ATP synthase in the inner membrane [Jeppesen et al., 2005]. Electron Transfer Flavoprotein is responsible for electron shuttles between primary flavoprotein dehydrogenases involved in mitochondrial fatty acid and amino acid catabolism and the membrane-bound electron transfer flavoprotein ubiquinone oxidoreductase [Roberts et al., 1996]. The change of these proteins suggested the dysfunction of mitochondria directly by MB-PDT.

With regard to ROS generation and removal, reduction of peroxiredoxin 3 isoform b and increase of peroxiredoxin 6 implicated that the extrinsic ROS produced by MB-PDT may destroy the balance of ROS in cells. Peroxiredoxin 3 isoform b was synthesized with a mitochondrial targeting sequence, as was MnSOD, and was then transferred to mitochondria [Chang et al., 2004]. The proteomic data showed that peroxiredoxin 3 isoform b is

TABLE I. Protein List of Differentially Expressed Proteins in MB-PDT Treatment

Spot no.	Accession no.[a]	Protein name	Ratio to the control			
			5 M	10 M	15 M	20 M
UP[b]						
1852	gi|56206057	Guanine nucleotide binding protein (G protein), alpha inhibiting activity polypeptide 3 [*Homo sapiens*]	0.84	1.04	0.77	1.64
1902	gi|58476967	HNRPC protein [*Homo sapiens*]	0.24	1.24	2.08	1.10
1972	gi|178438	Phosphatase 2A	1.31	0.81	1.00	1.27
1977	gi|47123412	RPLP0 protein [*Homo sapiens*]	0.58	1.17	1.37	1.33
2021	gi|62896495	Ribosomal protein P0 variant [*Homo sapiens*]	1.10	1.23	1.05	1.38
2103	gi|21594294	PITPNB protein [*Homo sapiens*]	0.70	0.33	1.54	1.75
2240	gi|18276665	Eukaryotic translation initiation factor 4H (eIF-4H) (Williams-Beuren syndrome chromosome region 1	1.17	0.74	1.03	1.45
2252	gi|33875631	ANP32A protein [*Homo sapiens*]	1.04	1.02	1.12	1.33
2307	gi|6018458	6-Phosphogluconolactonase [*Homo sapiens*]	0.80	0.65	0.63	1.98
2370	gi|56204402	Peroxiredoxin 6 [*Homo sapiens*]	0.28	1.38	1.03	1.87
2431	gi|6435686	Chain A, crystal structure of human Rhoa complexed with the effector domain of the protein kinase PknPRK1	1.08	0.99	1.22	1.06
2435	gi|21707709	Progesterone receptor membrane component 1 [*Homo sapiens*]	0.86	1.36	0.83	1.27
2440	gi|21707709	Progesterone receptor membrane component 1 [*Homo sapiens*]	0.81	1.31	1.02	1.18
2443	gi|30311	Cytokeratin 18 (424 AA) [*Homo sapiens*]	0.88	0.89	1.07	1.67
2481	gi|33991637	MGC15429 protein [*Homo sapiens*]	0.88	1.07	0.87	1.64
2519	gi|56417681	Splicing factor, arginine∨serine-rich 3 [*Homo sapiens*]	0.76	0.67	0.99	2.06
2587	gi|251371	Acid phosphatase isoenzyme Cf [human, erythrocytes, Peptide, 157 aa]	0.79	0.89	0.72	2.00
2603	gi|55961069	Prefoldin 2 [*Homo sapiens*]	0.93	1.02	0.91	1.55
2607	gi|42490908	Ras homolog enriched in brain [*Homo sapiens*]	0.80	0.59	1.01	1.91
2673	gi|6730223	Chain D, crystal structure of human profilin Ii	0.61	1.02	0.64	2.31
2681	gi|458862	Heart fatty acid binding protein; hFABP [*Homo sapiens*]	1.06	1.11	0.91	1.27
2713	gi|2506906	GTP cyclohydrolase I feedback regulatory protein (GFRP) (p35)	0.78	0.23	1.57	1.77
Down[c]						
836	gi|16356661	NRAS-related protein [*Homo sapiens*]	2.07	0.57	0.45	0.71
1101	gi|1082886	Tumor necrosis factor type 1 receptor associated protein TRAP-1-human	0.78	0.36	0.38	0.42
1383	gi|10280560	Succinyl-CoA:3-ketoacid CoA transferase [*Homo sapiens*]	0.96	0.92	0.77	0.66
1698	gi|899285	Mitochondrial elongation factor Tu [*Homo sapiens*]	1.01	0.73	0.65	0.51
1803	gi|45594399	CTD-like phosphatase domain-containing protein [*Homo sapiens*]	1.49	0.85	1.18	0.35
1887	gi|55959292	Annexin A1 [*Homo sapiens*]	0.83	0.79	0.69	0.47
1897	gi|10241724	Hypothetical protein [*Homo sapiens*]	1.03	0.32	0.54	0.96
2161	gi|625039	Elongation factor Ts	0.78	1.14	0.43	0.65
2203	gi|2781202	Chain A, three-dimensional structure of human electron transfer flavoprotein to 2.1 Å resolution	0.49	0.84	0.72	0.69
2447	gi|32483377	Peroxiredoxin 3 isoform b [*Homo sapiens*]	1.34	0.51	0.49	1.00
2589	gi|37183345	FKVI1866 [*Homo sapiens*]	1.09	0.65	1.26	0.00

HeLa cells were treated with MB-PDT (5, 10, 15, 20 M) or PDT alone. Light alone treated cells were used as control. Cells were collected 6 h after PDT. All proteins were identified using MALDI-TOF peptide mass fingerprinting.
[a]NCBI accession number.
[b]Up-regulated proteins.
[c]Down-regulated proteins.

up-regulated to 1.34 (contrast to the control) with 5 M MB, but down-regulated to about 0.5 with 10 or 15 M MB, and go back to 1 with 20 M MB. The possibility of this protein expression fluctuation may be related with alternative location of peroxiredoxin 3 isoform b and the effect of oxidant stress on antioxidant enzyme expression. However, peroxiredoxin 6 protein was found in cytosol, but not in membranes, organelles, and nuclei fractions. The antioxidant property of peroxiredoxin 6 was attributed to its ability to reduce H_2O_2 and alkyl hydroperoxide to water and alcohol, respectively [Wang et al., 2003].

TRAP1 is a member of the molecular chaperone HSP90 (90-kDa heat shock protein) family with a mitochondrial localization sequence at its N-terminus. It acts as an antagonist of ROS and protects mitochondria against damaging stimuli [Felts et al., 2000; Hua et al., 2007]. The decreased expression of TRAP1 by MB-PDT along with the accumulation of ROS in mitochondria suggested that TRAP1 is an effector target of MB. All these data indicated that MB-PDT treatment induces a large scale of extrinsic ROS, the dysfunction of mitochondria was caused by altering the structure and function of protein in mitochondria induced by ROS, and that the accumulated effect induced HeLa cells to undergo apoptosis through the mitochondria pathway.

Proteomic analyses showed that Gi3, ANP32A protein, phosphatase 2A were increased in MB-PDT treated cells. These proteins regulate downstream proteins. ANP32A protein suppresses the activation of ERK1/2 by activating PP2A [Yu et al., 2004]; Gi3 decrease cAMP and PKA activity [Valenti et al., 1998]. In non-apoptotic cells, ERK1/2 can phosphorylate and activate the 90 kDa ribosomal S6 kinase (p90RSK), which then leads to the phosphorylation and inactivation of Bad [Koh, 2007]. PKA directly phosphorylates many Serine residues of Bad. Phosphorylated Bad binds to 14-3-3 proteins in the cytoplasm and is trapped in cytoplasm. As a result, its binding to Bcl-xL is blocked and cells survive. However, in the apoptotic process phosphorylation of Bad was decreased as a result of the stimulation of apoptosis signal. Dephosphorylation of Bad inhibited the pro-survival function of Bcl-xL by binding with Bcl-xL and releasing Bax/Bak complex from Bcl-xL. The activation of Bax leads to the formation of Bax tetramer

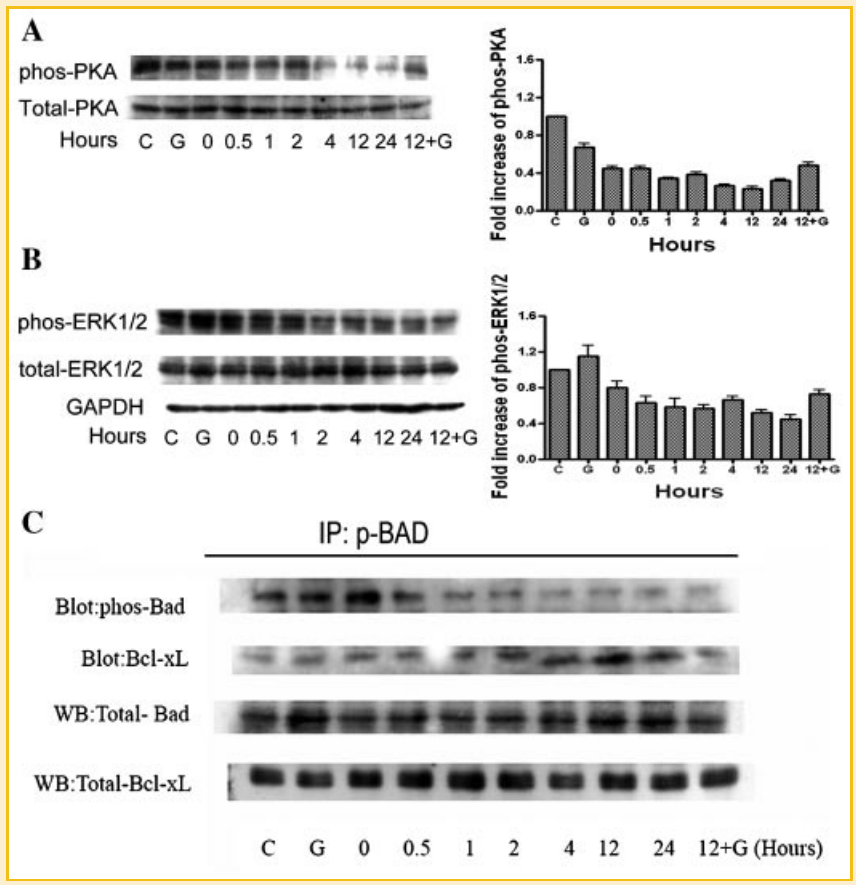

Fig. 4. MB-PDT-induced apoptosis is associated with MAPK/PKA and Bcl-2 family Western blotting analysis was performed to detect phosphorylated PKA, total PKA (A), phosphorylated ERK1/2 and total ERK1/2 (B), respectively. GAPDH severed as internal standard. C: Co-Immunoprecipitation was performed to determine the interaction between Bad and Bcl-xL in the apoptotic process. Cell lysates were incubated with anti-Bad antibody. The total expression of Bad and Bcl-xL were determined by Western blotting. The figures are representative of at least three separate experiments.

which penetrates mitochondrion membrane and induces the release of cytochrome *c*, and subsequent series of caspase reactions and the apoptosis [Downward, 1999; Cory and Adams, 2002; Chiang et al., 2003; Won et al., 2003].

We also used Western blotting and co-immunoprecipitation to investigate proteins regulating signal transduction pathway in MB-PDT induced apoptosis. The results suggested that MB-PDT induced down-regulation of a series of phosphorylated proteins, ERK1/2 and PKA, resulted in up-regulation of dephosphorylated Bad (phosphorylated Bad reduced and total Bad constant in Fig. 3C). Next, increased association of Bad with Bcl-xL released Bax/Bak complex from Bcl-xL (based on total Bcl-xL constant in Fig. 3) and brought on rapid release of cytochrome *c*. Addition of GSH could promote the phosphorylation of ERK1/2 and PKA that was previously suppressed by MB-PDT, restrain the release of cytochrome *c* and the cleavage of PARP. All these observations are consistent with the hypothesis that MB-PDT induces ROS and the consequent apoptosis in cells.

We confirmed the possibility that MB-PDT induces apoptosis by activating the intrinsic apoptosis pathway. First, we demonstrated that cytochrome *c* released from mitochondria to cytoplasm, a hallmark of initiation of mitochondria mediated apoptosis pathway. Meanwhile, MB-PDT treated cells showed enhanced activation of caspase-3, which is downstream of cytochrome *c* and associated with elevated cleavage of PARP [Carmen and Guido, 2004]. Furthermore, the loss of mitochondrial membrane potential () in the dose-dependent manner presented in our study provided crystal evidence of the intrinsic apoptosis. By performing a variety of analyses on HeLa cells treated by MB-PDT, we delineated a series of molecular events that took place upon the treatment, established that MB-PDT can induce the mitochondria-mediated apoptosis.

In conclusion, our results support the hypothesis that MB-PDT generates ROS and induces up-regulation of several proteins that are essential in the regulation of apoptosis. This in turn inhibits the activity of protein kinase such as PKA, ERK1/2. The inhibition eventually stimulates the down-regulation of phosphorylated Bad and the increase of Bcl-xL bound with Bad. The protective function of Bcl-xL is blocked through its association with Bad. The destroyed mitochondria release cytochrome *c*, initiate incision of PARP and induce apoptosis consequently. The hypothetical model of the apoptotic pathway in HeLa cells upon PDT treatment with MB is shown in Figure 5.

Our studies demonstrate that MB-PDT triggers apoptosis through mitochondrial-mediated mechanisms and selective modulation of

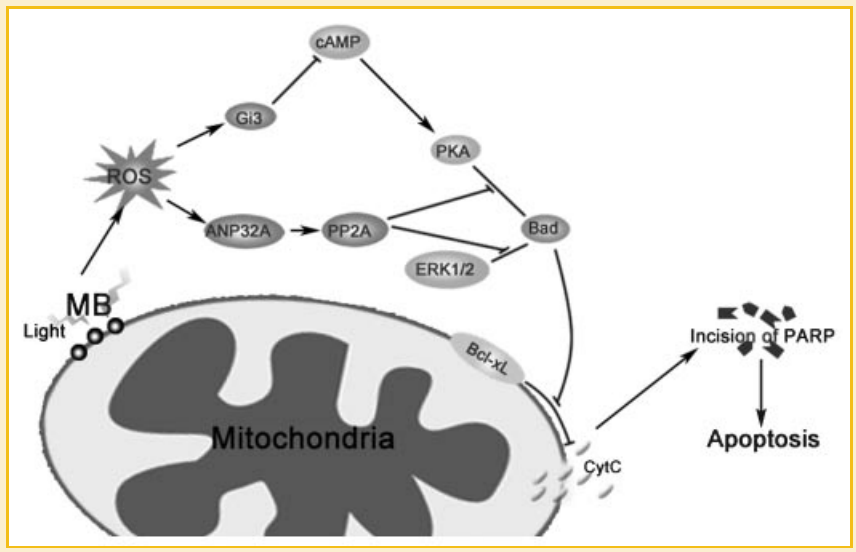

Fig. 5. The hypothetical models of apoptosis pathway in HeLa cell response to PDT treatment with MB.

the mitochondrial redox equilibrium. Understanding the multiple molecular events involved in the process will shed light on the exploration of drug targets in mitochondria for improved therapeutic approaches by MB-PDT. Reconstruction of MB, methylene blue derivative and methylene blue-containing nano particles to have high phototoxicity at low light dose may facilitate the application of photosensitizer to clinical therapy.

MATERIALS AND METHODS

REAGENTS

The photosensitizer methylene blue (MB) used for PDT was acquired from Aldrich (Milwaukee, WI). RPMI 1640 medium was supplied by Hyclone (Logan, UT). Antibodies against cytochrome *c*, PARP, GAPDH, PKA, ERK1/2, p-Bad, Bcl-xl and caspase-3 were purchased from Cell Signaling Technology (Beverly, MA). All chemicals were purchased from Sigma Chemicals (St. Louis, MO) unless otherwise stated.

CELL CULTURE AND PDT TREATMENT

HeLa cells (Shanghai Institutes for Biological Sciences, Chinese Academy of Sciences, Shanghai, China) were seeded at 5×10^4 cells per cm^2 in RPMI-1640 with 10% FCS, 100 units/ml Penicillin and 100 units/ml Streptomycin. Cells grown to 80–90% confluence were treated with MB-PDT. Briefly, HeLa cells were incubated for 1 h in serum-free medium containing different doses of MB (ranging from 0 to 20 M) for 1 h at 37°C. This medium was then removed and replaced with fresh complete medium. Then the cells were irradiated with 650-nm light produced by a dye laser (Red Diode Laser, Tianjin GangDong Technical Co. Ltd., China) at 10 J/cm^2 for 30 min with 30 s intermission at 15 min. After the indicated time, cells were collected and subjected to assays. The test of MB without environmental illumination was finished in darkroom or covered with aluminum foil to avoid the light.

MEASUREMENT OF APOPTOSIS

Cell apoptosis was measured with the DNA dye 7-AAD. For 7-AAD assays, HeLa cells transfected with various constructs at different time points were detached from the tissue culture plates with 0.25% trypsin–EDTA, washed, and then incubated for 10 min with 7-AAD (5 l per tube). Flow cytometry acquisition was performed immediately after the incubation, and the percentage of 7-AAD positive cells was determined using CellQuest™ software. To confirm morphological changes in the nuclei, cells were seeded in 60-mm dishes at a concentration of 5×10^5 cells/ml.

With different dose of MB-PDT for 24 h, cells were incubated for 30 min in the presence of 20 g/ml Hoechst 33258 and then examined by fluorescence microscopy (Olympus, Tokyo, Japan). Hoechst stain and Annexin V-FITC/PI flow cytometry were adapted from reference [Cordoba et al., 2005]. Please refer to SI methods for further details of the procedure used in this work.

WESTERN BLOT

The following antibodies were used for Western blot analysis, including, and anti-cytochrome *c*, anti-PARP, anti-GAPDH, anti-PKA, anti-ERK1/2, anti-p-Bad, anti-Bad, anti-Bcl-xl. The extracted proteins of HeLa cells treated as above were separated by SDS–PAGE and electrophoretically transferred to PVDF membranes (Amersham Biosciences). After being blocked for 4 h, the membranes were incubated with antibodies overnight at 4°C, and then with horseradish peroxidase-labeled goat anti-rabbit IgG for 2 h. The blots were visualized with an enhanced chemiluminescent method kit (SABC, PRC).

MITOCHONDRIAL MEMBRANE POTENTIAL ($\Delta\psi$) ASSAY

To assess the mitochondrial membrane potential (), the green-fluorescent lipophilic cationic dye DiOC6 (Molecular Probes) was used. HeLa Cells (1×10^6) from various treated groups were trypsinized and washed with cold PBS twice. They were then

resuspended in 400 l medium and cultured in 20 nM DiOC6 at 37°C for 30 min. Mitochondrial membrane potential was determined by FACS analysis using a Becton Dickinson FACSCalibur.

EFFECT OF INTRACELLULAR ROS ON CELL DEATH

The generation of intracellular ROS was detected by using the fluorescence probe DCFH-DA (Marker Gene) and DHR123 (Marker Gene). In DCFH-DA method, Cells were plated in a 96-well plate (1×10^5 cells/well). After 24 h, HeLa cells were incubated in 10 M DCFH-DA for 20 min at 37°C followed by the addition of different concentrations of MB. Cells were then irradiated for 30min or not. The quantification of fluorescence intensity was analyzed by a microplate reader after irradiation. The percentage of cell death was determined by 7-AAD staining in the presence or absence of antioxidant GSH (50 mM), respectively. In DHR123 method, Cells were plated in a 96-well plate (1×10^5 cells/well). After 24 h, cells were incubated in 5 M DHR123 for 1 h at 37°C. Then different concentrations of MB were added to cultures, which were irradiated for 30 min. Fluorescence was photographed by using a fluorescent Mutilabel Counter (Safire, TECAN, Austria) and quantified by excitation at 488 nm and emission at 530 nm.

PROTEOMICS

HeLa cells were treated with MB-PDT (5, 10, 15, 20 M) or PDT without MB. Light alone treated cells were used as control. Cells were collected 6 h after PDT. Two-dimensional gel electrophoresis was carried out with Amersham Biosystems IPGphor IEF and Hoefer Tank (13 cm) units, in accordance with a previously described protocol [Zhou et al., 2004; Xie et al., 2008]. Protein samples were used for two-dimensional gel electrophoresis analysis. Triplicate electrophoresis was done to ensure reproducibility. All gels were visualized by CBB R-250.

After staining, the gels were scanned with Powerlook 2100 XL Scanner (Umax, Dallas) with 400 dpi and images were analyzed with PDQuest V7.3.0 software (Bio-Rad, Hercules). Comparisons were made between gel images of cells treated with various MB-PDT and the PDT alone control. Altered protein spots that changed consistently and significantly (>2-fold difference) were selected for analysis with Ultraflex matrix-assisted laser desorption/ionization-time of flight (MALDI-TOF) mass spectrometry (Bruker Daltonics, Bremen, Germany). The protein identification was performed by peptide mass fingerprinting using the database search program MASCOT (Matrix Science, Boston). The searching parameters were set as follows: taxonomy—*Mus musculus*; database—SwissProt or NCBInr, release 20041123/no. Duplicate or triplicate runs were made to ensure the accuracy of the analysis.

CO-IMMUNOPRECIPITATION

Co-immunoprecipitation was performed to determine the interaction between Bad and Bcl-xL in the apoptotic process. Two microliters of anti-Bad was added to the Cell lysates in 4°C. After 4 h, 50 l of protein A-agarose (Protein A agarose suspension, Calbiochem, Germany) was again added and incubated for 1 h. The agarose beads were then washed four times with 500 l of RIPAE buffer (150 mM NaCl, 1.0% NP-40, 2 mM EDTA, 50 mM Tris–HCl [pH 8.0]). The pellets were heated to 100°C for 5 min and subjected to SDS–PAGE gel separation. The p-Bad and Bcl-xL combined with Bad were detected by anti p-Bad and anti Bcl-xL blots respectively in two independent experiments. The total expression of p-Bad and Bcl-xL were determined by Western blotting. GAPDH was used as an internal standard. The figures are representative of at least three independent experiments.

STATISTICAL ANALYSIS

Data were statistically evaluated by Student's *t*-test when only two value sets were compared, or one-way ANOVA followed by Dunnett's test when three or more groups were present. Results were expressed as mean $\pm$ SD. $P < 0.05$ or $P < 0.01$ was considered statistically significant and indicated by * or **, respectively.

ACKNOWLEDGMENTS

This work was supported by the Program for New Century Excellent Talents in University NCET-06-0445 and grants from National Basic Research Program of China No. 2006CB910103. We thank Xiaolu L. Ang (Harvard University) for grammatical correction of the manuscript.

REFERENCES

Almeida RD, Manadas BJ, Carvalho AP, Duarte CB. 2004. Intracellular signaling mechanisms in photodynamic therapy. Biochim Biophys Acta 1704:59–86.

Ball DJ, Luo Y, Kessel D, Griffiths J, Brown SB, Vernon DI. 1998. The induction of apoptosis by a positively charged methylene blue derivative. J Photochem Photobiol B 42:159–163.

Bellin JS, Mohos SC, Oster G. 1961. Dye-sensitized photoinactivation of tumor cells in vitro. Cancer Res 21:1365–1371.

Buytaert E, Dewaele M, Agostinis P. 2007. Molecular effectors of multiple cell death pathways initiated by photodynamic therapy. Biochim Biophys Acta 1776:86–107.

Carmen G, Guido K. 2004. Life's smile, death's grin: Vital functions of apoptosis-executing proteins. Curr Opin Cell Biol 16:639–646.

Chang TS, Cho CS, Park S, Yu S, Kang SW, Rhee SG. 2004. Peroxiredoxin III, a mitochondrion-specific peroxidase, regulates apoptotic signaling by mitochondria. J Biol Chem 279:41975–41984.

Chiang CW, Kanies C, Kim KW, Fang WB, Parkhurst C, Xie MH, Henry T, Yang E. 2003. Protein phosphatase 2A dephosphorylation of phosphoserine 112 plays the gatekeeper role for BAD-mediated apoptosis. Mol Cell Biol 23:6350–6362.

Cordoba F, Braathen LR, Weissenberger J, Vallan C, Kato M, Nakashima I, Weis J, von Felbert V. 2005. 5-aminolaevulinic acid photodynamic therapy in a transgenic mouse model of skin melanoma. Exp Dermatol 14:429–437.

Cory S, Adams JM. 2002. The Bcl2 family: Regulators of the cellular life-or-death switch. Nat Rev Cancer 2:647–656.

Dolmans DE, Fukumura D, Jain RK. 2003. Photodynamic therapy for cancer. Nat Rev Cancer 3:380–387.

Dougherty TJ, Gomer CJ, Henderson BW, Jori G, Kessel D, Korbelik M, Moan J, Peng Q. 1998. Photodynamic therapy. J Natl Cancer Inst 90:889–905.

Downward J. 1999. How BAD phosphorylation is good for survival. Nat Cell Biol 1:33–35.

Felts SJ, Owen BAL, Nguyen P, Trepel J, Donner DB, Toft DO. 2000. The hsp90-related protein TRAP1 is a mitochondrial protein with distinct functional properties. J Biol Chem 275:3305–3312.

Furre IE, Shahzidi S, Luksiene Z, Møller MT, Borgen E, Morgan J, Tkacz-Stachowska K, Nesland JM, Peng Q. 2005. Targeting PBR by hexaminolevulinate-mediated photodynamic therapy induces apoptosis through translocation of apoptosis-inducing factor in human leukemia cells. Cancer Res 65:11051–11060.

Gabrielli D, Belisle E, Severino D, Kowaltowski AJ, Baptista MS. 2004. Binding, aggregation and photochemical properties of methylene blue in mitochondrial suspensions. Photochem Photobiol 79:227–232.

Gill WB, Taja A, Chadbourne DM, Roma M, Vermeulen CW. 1987. Inactivation of bladder tumor cells and enzymes by methylene blue plus light. J Urol 138:1318–1320.

Henderson BW, Doughterty TJ. 1992. How does photodynamic therapy work? Photochem Photobiol 55:145–157.

Hopper C. 2000. Photodynamic therapy: A clinical reality in the treatment of cancer. Lancet Oncol 1:212–219.

Horbinski C, Chu CT. 2005. Kinase signaling cascades in the mitochondrion: A matter of life or death. Free Radic Biol Med 38:2–11.

Hua G, Zhang Q, Fan Z. 2007. Heat shock protein 75 (TRAP1) antagonizes reactive oxygen species generation and protects cells from granzyme M-mediated apoptosis. J Biol Chem 282:20553–20560.

Jeppesen MG, Navratil T, Spremulli LL, Nyborg J. 2005. Crystal structure of the bovine mitochondrial elongation factor Tu–Ts complex. J Biol Chem 280:5071–5081.

Kirszberg C, Rumjanek VM, Capella MAM. 2005. Methylene blue is more toxic to erythroleukemic cells than to normal peripheral blood mononuclear cells: A possible use in chemotherapy. Cancer Chemother Pharmacol 55:659–665.

Klumpp S, Krieglstein J. 2002. Serine/threonine protein phosphatases in apoptosis. Curr Opin Pharmacol 2:458–462.

Koh PO. 2007. Estradiol prevents the injury-induced decrease of 90 ribosomal S6 kinase (p90RSK) and Bad phosphorylation. Neurosci Lett 412:68–72.

Manyak MJ, Russo A, Smith PD, Glatstein E. 1998. Photodynamic therapy. J Clin Oncol 6:380–391.

Noodt BB, Rodal GH, Wainwright M, Peng Q, Horobin R, Nesland JM, BERG K. 1998. Apoptosis induction by different pathways with methylene blue derivative and light from mitochondrial sites in V79 cells. Int J Cancer 75:941. 948.

Orth K, Beck G, Genze F, Ruck A. 2000. Methylene blue mediated photodynamic therapy in experimental colorectal tumors in mice. J Photochem Photobiol B 57:186–192.

Reynolds T. 1997. Photodynamic therapy expands its horizons. J Natl Cancer Inst 89:112–114.

Roberts DL, Frerman FE, Kim JJP. 1996. Three-dimensional structure of human electron transfer flavoprotein to 2.1-Å resolution. Proc Natl Acad Sci 93:14355–14360.

Rodrigues T, de Franca LP, Kawai C, de Faria PA, Mugnol KCU, Braga FM, Tersariol ILS, Smaili SS, Nantes IL. 2007. Protective role of mitochondrial unsaturated lipids on the preservation of the apoptotic ability of cytochrome c exposed to singlet oxygen. J Biol Chem 282:25577–25587.

Schmidt S, Schultes B, Wagner U, Oehr P, Decleer W, Lubaschowski H, Biersack HJ, Krebs1 D. 1991. Photodynamic laser therapy of carcinomas–Effects of five different photosensitizers in the colony-forming assay. Arch Gynecol Obstet 249:9–14.

Tardivo JP, Giglio AD, Oliveira CSD, Gabrielli SD, Junqueira HC, Tada DB, Severinob D, Turchiellob RdF, Mauricio S, Baptista PhD. 2005. Methylene blue in photodynamic therapy: From basic mechanisms to clinical applications. Photodiagn Photodyn Therapy 2:175–191.

Tuite EM, Kelly JM. 1993. Photochemical interactions of methylene blue and analogues with DNA and other biological substrates. J Photochem Photobiol B 21:103–124.

Vakkila J, Lotze MT. 2004. Inflammation and necrosis promote tumour growth. Nat Rev Immunol 4:641. 648.

Valenti G, Procino G, Liebenhoff U, Frigeri A, Benedetti PA, Ahnert-Hilger G, Nürnberg B, Svelto M, Rosenthal W. 1998. A heterotrimeric G protein of the Gi family is required for cAMP-triggered trafficking of aquaporin 2 in kidney epithelial cells. J Biol Chem 273:22627–22634.

Vantieghem A, Xu Y, Assefa Z, Piette J, Vandenheede JR, Merlevede W, de Witte PAM, Agostinis P. 2002. Phosphorylation of Bcl-2 in G2/M phase-arrested cells following photodynamic therapy with hypericin involves a CDK1-mediated signal and delays the onset of apoptosis. J Biol Chem 277:37718–377313.

Wang X, Phelan SA, Forsman-Semb K, Taylor EF, Petros C, Brown A, Lerner CP, Paigen B. 2003. Mice with targeted mutation of peroxiredoxin 6 develop normally but are susceptible to oxidative stress. J Biol Chem 278:25179–25190.

Waterhouse NJ, Goldstein JC, Ahsen OV, Schuler M, Newmeyer DD, Green DR. 2001. Cytochrome c maintains mitochondrial transmembrane potential and ATP generation after outer mitochondrial membrane permeabilization during the apoptotic process. J Cell Biol 153:319–328.

Won J, Kim DY, La M, Kim D, Meadows GG, Joe CO. 2003. Cleavage of 14-3-3 protein by caspase-3 facilitates bad interaction with Bcl-x(L) during apoptosis. J Biol Chem 278:19347–19351.

Xie X, Li S, Liu S, Lu Y, Shen P, Ji J. 2008. Proteomic analysis of mouse islets after multiple low-dose streptozotocin injection. Biochim Biophys Acta 784:276–284.

Yao J, Zhang GJ. 1996. Loss of lysosomal integrity caused by the decrease of proton translocation in methylene blue-mediated photosensitization. Biochim Biophys Acta 1284:35–40.

Yu L, Packman LC, Weldon M, Hamlett J, Rhodes JM. D 2004. Protein phosphatase 2A, a negative regulator of the ERK signaling pathway, is activated by tyrosine phosphorylation of putative HLA class II-associated protein I (PHAPI)/pp32 in response to the antiproliferative lectin, jacalin. J Biol Chem 279:41377–41383.

Zhang LZ, Tang GQ. 2005. The binding properties of photosensitizer methylene blue to herring sperm DNA: A spectroscopic study. J Photochem Photobiol B 74:119–125.

Zhou B, Yang W, Ji JG, Ru BG. 2004. Differential display proteome analysis of PC-12 cells transiently transfected with metallothionein-3 gene. J Proteome Res 3:126–131.